Ring bursting behavior en route to turbulence in quasi two-dimensional Taylor-Couette flows

Sebastian Altmeyer,[1,*] Younghae Do,[2,†] and Ying-Cheng Lai[3]

[1]*Institute of Science and Technology Austria, 3400 Klosterneuburg, Austria*
[2]*Department of Mathematics, KNU-Center for Nonlinear Dynamics, Kyungpook National University, Daegu, 702-701, Korea*
[3]*School of Electrical, Computer and Energy Engineering, Arizona State University, Tempe, Arizona 85287, USA*

(Dated: January 12, 2015)

We investigate the quasi two-dimensional Taylor-Couette system in the regime where the radius ratio is close to unity - a transitional regime between three and two dimensions. By systematically increasing the Reynolds number we observe a number of standard transitions, such as one from the classical Taylor vortex flow (TVF) to wavy vortex flow (WVF), as well as the transition to fully developed turbulence. Prior to the onset of turbulence we observe intermittent burst patterns of localized turbulent patches, confirming the experimentally observed pattern of very short wavelength bursts (VSWBs). A striking finding is that, for Reynolds number larger than the onset of VSWBs, a new type of intermittently bursting behaviors emerge: burst patterns of azimuthally closed rings of various orders. We call them *ring-burst* patterns, which surround the cylinder completely but remain localized and separated by non-turbulent mostly wavy structures in the axial direction. We use a number of quantitative measures, including the cross-flow energy, to characterize the ring-burst patterns and to distinguish them from the background flow. The ring-burst patterns are interesting because it does not occur in either three- or two-dimensional Taylor-Couette flow: it occurs only in the transition, quasi two-dimensional regime of the system, a regime that is less studied but certainly deserves further attention so as to obtain deeper insights into turbulence.

PACS numbers: 47.20.Ky, 47.32.cf, 47.54.-r

I. INTRODUCTION

Characteristics of turbulence in three- and two-dimensional flows are typically quite distinct. For example, in three-dimension flows, the energy spectrum of fully-developed turbulence obeys the well-known Kolmogorov 1941 scaling law [1] of $k^{-5/3}$, while in two dimensions the scaling [2, 3] is k^{-3}. Although two-dimensional flow systems offer great advantages from the standpoint of computation and mathematical analysis as compared with three-dimensional flows, the former are not merely a kind of toy model of turbulence. In fact, two-dimensional turbulence is relevant to the dynamics of oceanic currents, origin of the ozone hole through mixing of chemical species in the polar stratosphere, the existence of polar vortex, strong eddy motions such as tropical cyclones, and other large-scale motions of planetary atmospheres [4, 5].

Turbulence is arguably one of the most difficult problems in science and engineering, and the vast literature on turbulence was mostly focused on three or two dimensions [6]. To gain new insights into turbulence, it is of interest to study the *transitional regime* between three and two dimensions. In such a regime, properties of both three- and two-dimensional flows are relevant, and one naturally wonders whether there are any unexpected features associated with, for instance, transition to turbulence [7, 8]. The purpose of this paper is to report a new phenomenon in a paradigmatic quasi-two-dimensional system: the Taylor-Couette flow [9] with gap between the inner and outer cylinders so narrow that the system is neither completely three-dimensional nor exactly two-dimensional. In fact, this regime has not been investigated systematically previously. The new type of intermittent dynamics occurs *en route* to turbulence as the Reynolds number is increased.

The Taylor-Couette system, a flow between two concentric rotating cylinders, has been a paradigm in the study of complex dynamical behaviors of fluid flows, especially turbulence [10–18]. The flow system can exhibit a large variety number of ordered and disordered behaviors in different parameter regimes. For cylinders of reasonable length, the effective dimensionality of the system is determined by a single parameter - the ratio between the radii of the two cylinders. If the ratio is markedly less than unity, the flow is three dimensional. As the ratio approaches unity, the flow becomes two dimensional.

*Electronic address: sebastian.altmeyer@ist.ac.at
†Electronic address: yhdo@knu.ac.kr

Most previous studies focused on the setting where the radius ratio is below, say about 0.9, the so-called wide-gap regime [13], or when the ratio approaches unity so that the geometry is locally planar, resulting in an effectively two-dimensional Couette flow [19]. Here, we are interested in the narrow-gap case, where the radius ratio is close to unity but still deviates from it so that the flow is quasi two-dimensional. To be concrete, we fix the radius ratio to be 0.99 and, without loss of generality, restrict our study to the case where the outer cylinder is stationary. In fact, regardless of whether the outer cylinder is rotational or stationary, transition to turbulence can occur with increasing Reynolds number. In particular, for systems of counter-rotating cylinders, an early work [10] showed that transition to turbulence can be sudden as the Reynolds number is increased through a critical point. For fixed outer cylinder, the transition from laminar flow to turbulence can occur through a sequence of instabilities of distinct nature [14, 20].

For Taylor-Couette system of counter-rotating cylinders, spatially isolated flow patterns, the so-called localized patches, can emerge through the whole fluid domain and decay [13, 21]. Depending on the parameters, the localized patches can be laminar or more complex patterns such as inter-penetrating spirals. In the wide-gap regime (three-dimensional flow), numerical simulations [22] revealed the existence of so-called Görtler vortices [23], small scale azimuthal vortices that can cause streaky structures and form herringbone-like patterns near the wall. Localized turbulent behaviors can arise when the Görtler vortices concentrate and grow at the outflow boundaries of the Taylor vortex cell [22].

For narrow gap (quasi two-dimensional) flows, there was experimental evidence of the phenomenon of very short wavelength bursts (VSWBs) [14]. One contribution of our work is clear computational demonstration of VSWBs. Remarkably, we uncover a class of solutions in quasi two-dimensional Taylor-Couette flow *en route* to turbulence. These are localized, irregular, intermittently bursting, azimuthally closed patterns that manifest themselves as various rings located along the axial direction. For convenience, we refer to the states as "*ring-bursts*." The number of distinct rings can vary depending on the parameter setting but their extents in the axial direction are similar. The ring bursts can occur on some background flow that is not necessarily regular. For example, in typical settings the background can be wavy vortex flows (WVFs) with relatively high azimuthal wave numbers. Because of the coexistence of complex flow patterns, to single out ring bursts is challenging, a task that we accomplish by developing an effective mode separation method based on the cross-flow energy. We also find that ring bursts are precursors to turbulence, *signifying a new route to turbulence* uniquely for quasi two-dimensional Taylor-Couette flows. To our knowledge, there was no prior report of ring bursts patterns or likes. This is mainly due to the fact that the quasi two-dimensional regime is a less explored territory in the giant landscape of turbulence research. It would be interesting to identify precursors to turbulence in quasi two-dimensional flow systems in general.

In Sec. II, we outline our numerical method and describe a number of regular states in quasi two-dimensional Taylor-Couette flows. In Sec. III, we present our main results: numerical confirmation of experimentally observed VSWBs and more importantly, identification and quantitative confirmation of intermittent ring bursts as precursors to turbulence. In Sec. IV, we present conclusions and discussions.

II. NUMERICAL METHOD AND BASIC DYNAMICAL STATES OF QUASI TWO-DIMENSIONAL TAYLOR-COUETTE FLOW

A. Numerical method

The Taylor-Couette system consists of two independently rotating cylinders of finite length L and a fluid confined in the annular gap between the two cylinders. We consider the setting in which the inner cylinder of radius R_i rotates at angular speed Ω and the outer cylinder of radius R_o is stationary. The end-walls enclosing the annulus in the axial direction are stationary and the fluid in the annulus is assumed to be Newtonian, isothermal and incompressible with kinematic viscosity ν. Using the gap width $d = R_o - R_i$ as the length scale and the radial diffusion time (DT) d^2/ν as the time scale, the non-dimensionalized Navier-Stokes and continuity equations are

$$\partial_t \boldsymbol{u} + (\boldsymbol{u}\cdot\nabla)\boldsymbol{u} = -\nabla p + \nabla^2 \boldsymbol{u}, \qquad \nabla\cdot\boldsymbol{u} = 0, \qquad (1)$$

where $\boldsymbol{u} = (u_r, u_\theta, u_z)$ is the flow velocity field in cylindrical coordinates (r, θ, z), the corresponding vorticity is given by $\nabla\times\boldsymbol{u} = (\xi, \eta, \zeta)$, and r is the normalized radius for fluid in the gap ($0 \le r \le 1$). The three relevant parameters are the Reynolds number $Re = \Omega_i R_i d/\nu$, the radius ratio $R_i/R_o = 0.99$, and the aspect ratio $\Gamma \equiv L/d = 44$. The boundary conditions on the cylindrical surfaces are of the non-slip type, with $\boldsymbol{u}(r_i, \theta, z, t) = (0, Re, 0)$, $\boldsymbol{u}(r_o, \theta, z, t) = (0, 0, 0)$, where the non-dimensionalized inner and outer radii are $r_i = R_i/d$ and $r_o = R_o/d$, respectively. The boundary conditions in the axial direction are $\boldsymbol{u}(r, \theta, \pm 0.5\Gamma, t) = (0, 0, 0)$.

We solve Eq. (1) by using the standard second-order

time-splitting method with consistent boundary conditions for the pressure [24]. Spatial discretization is done via a Galerkin-Fourier expansion in θ and Chebyshev collocation in r and z. The idealized boundary conditions are discontinuous at the junctions where the stationary end-walls meet the rotating inner cylinder. In experiments there are small but finite gaps at these junctions where the azimuthal velocity is adjusted to zero. To achieve accuracy associated with the spectral method, a regularization of the discontinuous boundary conditions is implemented, which is of the form

$$u_\theta(r,\theta,\pm 0.5\Gamma,t) = Re\{\exp([r_i - r]/\epsilon) + \exp([r - r_o]/\epsilon)\}, \quad (2)$$

where ϵ is a small parameter characterizing the physical gaps. We use $\epsilon = 6 \times 10^{-3}$. Our numerical method was previously developed to study the end-wall effects in the Taylor-Couette system with co- and counter-rotating cylinders [25, 26]. In the present work we use up to $n_r = 50$ and $n_z = 500$ Chebyshev modes in the radial and axial directions, respectively, and up to $n_\theta = 100$ Fourier modes in the azimuthal direction. The time step is chosen to be $\delta t = 10^{-6}$.

B. Qualitative description of basic dynamical states

1. Low order instabilities

In the wide-gap, three-dimensional Taylor-Couette system, various flow patterns and their bifurcation behaviors are relatively well understood [10, 13]. In our quasi two-dimensional setting, a number of known low-order, non-turbulent instabilities still occur, which constitute the background flow upon which a new type of ring burst structures emerge. Here we describe these low-order instabilities. To visualize and distinguish qualitatively different flow patterns, we use the contour plots of the azimuthal vorticity component η.

Primary instability - Taylor vortex flow. As the Reynolds number Re is increased, the basic state, circular Couette flow (CCF) becomes unstable and is replaced by the classical Taylor vortex flow (TVF) that consists of toroidally closed vortices. TVFs with some increasing numbers of vortices appear gradually over a large range of Re, starting from a single Taylor vortex cell generated by the mechanism of Ekman pumping near the end walls. This initial cell can appear either near the top or the bottom lid. In a perfectly circular geometry, initial Taylor vortex cells can occur simultaneously at both lids, but this is less likely in realistic systems due to the inevitable imperfections in the system. The onset of initial TVF cells was experimentally found for Re about [14] 358. We find, numerically, that the onset value is about 356. As Re is increased from this value, additional vortices appear, which enter the bulk from near the lids until they finally fill the whole annulus for Re value about 435 (experimentally the value is about [14] 437). For example, we observe a TVF with 22 pairs of vortices within the annulus, with the characterizing wavenumber of $k = 3.427$, and an additional pair of Ekman boundary layer vortices near the top and bottom lids.

Secondary instabilities - wavy vortex flow. Further increasing Re, the TVF becomes unstable and is replaced by wavy vortex flow (WVF), a kind of centrifugal instability that appears via a supercritical Hopf bifurcation, which exhibits a wavy-like modulation but the vortices remain azimuthally closed. We find that the onset of WVF occurs for $Re \approx 473$ (experimentally the value is about [14] 475). The WVF, as shown in Fig. 1(a), is associated with relatively *high* values of the azimuthal wave number m. In general, WVF states consisting of many azimuthal modes can occur. For example, the WVF pattern in Fig 1(a) contains $m = 39$ modes, which we name as WVF_{39}. We find that this particular WVF state is in fact a global background flow state in a wide range of Re values.

The TVF and WVF patterns occur regardless of whether the flow is three dimensional or quasi two-dimensional, although the critical values of Re for the onsets of these flow patterns depend on the system details.

2. High-order instabilities

Very short wavelength bursts and localized patches. For the commonly studied [13], wide-gap, three-dimensional Taylor-Couette system, e.g., of radius ratio 0.883, the typical sequence of solutions with increasing Re values is as follows. As the stationary TVF becomes unstable, time dependent WVF arises, followed by the so-called modulated WVF [13], eventually leading to turbulent behaviors. However, in the narrow-gap, quasi two-dimensional system, we have not observed the global transition from WVF to modulated WVF. Instead, we find that very short wavelength bursts (VSWBs) appear directly after the onset of WVF *without* any other types of intermediate solutions. Onset of VSWBs is $Re \approx 483$, which agrees with the experimentally observed onset value [14].

As Re is increased, we observe *localized patches* (LPs) superposed on WVF. The pattern within LPs can be either wavy-like or turbulent, depending on the Re value (lower and high values for the former and the latter, respectively). In particular, LPs with wavy-like interior behaviors emerge, and for $Re > 580$ LPs with turbu-

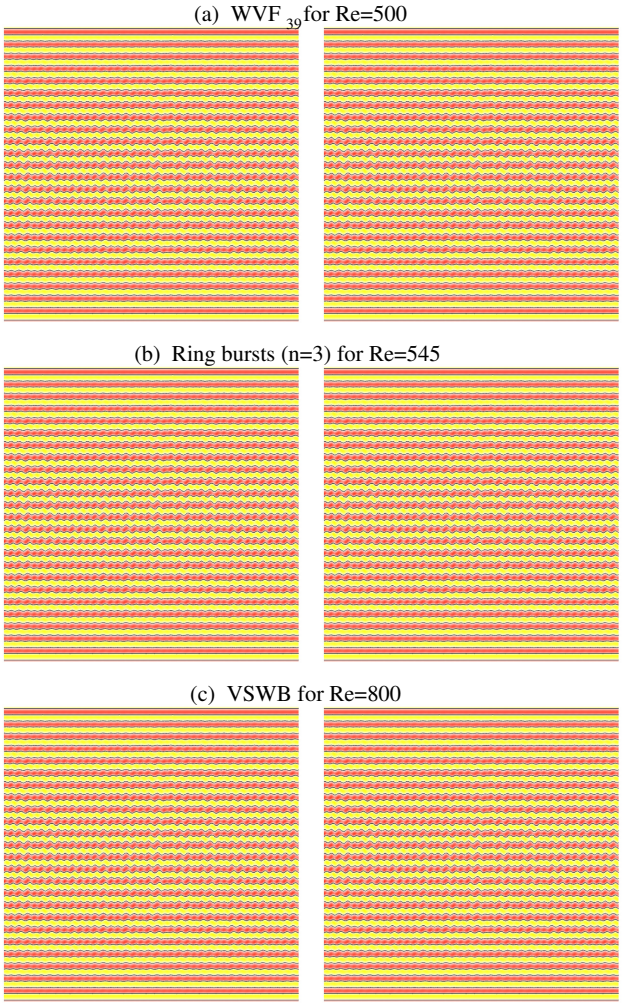

FIG. 1: (Color online) **Distinct flow patterns in quasi two-dimensional Taylor-Couette system.** Contours of the azimuthal vorticity component η with (left column, $\eta \in [-400, 400]$) and without (right column, $\eta(m \neq 0) \in [-200, 200]$) the axisymmetric component on an unrolled cylindrical surface at the midgap ($r = d/2$) for different flows and values of Re. Red (dark gray) and yellow (light gray) colors correspond to positive and negative values, respectively, and the black line indicates the zero contour.

lent behaviors arise, which can either grow to VSBWs or decay slowly. The number of LPs depends on Re as well. In general, the higher the value of Re the larger the number of LPs appears. The patches are randomly distributed over the whole bulk length and are always visible except for the region near the lids in which strong Ekman vortices arise.

Ring-burst patterns. When Re is increased above about 540, we discover a *new* type of localized, intermittent burst solution, the *ring bursts* that coexist with VSWBs. While both types of solutions are localized, there are characteristic differences. For example, VSWBs appear randomly over the whole bulk fluid region with seemingly expanding behaviors in all directions, but ring bursts always remain *localized* in the axial direction. In fact, the bursts are generated from the localized turbulent patches that grow in the azimuthal direction as Re is increased. For sufficiently high values of Re, the patches extend over one circumference, generating distinct ring bursts that are separated from the flow patterns in the rest of the bulk, as shown in Fig. 1(c). The characteristics of the background flows in the regions surrounding the ring bursts depend strongly on Re. They can range from wavy-like patterns (i.e., WVF_{39}) to interpenetrating spirals due to the interactions among various azimuthal modes, as shown in Fig. 1(c). We observe ring burst patterns of different order n, as shown in Figs. 1 and 2). For example, we observe $n \in \{1, 2, 3\}$. All these states coexist but the probability for ring bursts with larger values of n increases with Re. Along the axial direction, the ring burst patterns can appear at any position, except for the regions of Ekman vortices near the lids, because strong boundary layer vortices prevent the development of ring burst patterns.

While there is no apparent order associated with the flow patterns within the ring bursts, the flow in the regions in between exhibit a clear signature of WVF_{39} pattern. The ring bursts can spontaneously break up and disappear. Depending on the number of ring bursts, the transient time that it takes for the burst to decay into localized patches can be relatively long. In addition, there can be transitions between patterns with distinct numbers of ring bursts. For example, suppose there is a ring-burst pattern of order $n = 3$. If one ring disappears, a new ring-burst region can appear and grow. Transitions between patterns with either increasing or decreasing numbers of ring bursts have been observed.

For $Re > 850$, we find that VSWBs fill the whole bulk fluid region, as shown in Fig. 1(c). In fact, for $Re > 900$, the whole fluid region is saturated with VSWBs. These numerical observations are in agreement with experimental findings [14]. Note, however, even when VSWBs fill the interior of the bulk WVF-like patterns always appear near the axial end-walls due to the fact that Ekman vortices can stabilize the boundary layers against turbulent bursts. The size of the WVF-like Ekman regions depends on Re - for higher value of Re the smaller the WVF regions near the lids appear, as can be seen from Fig. 1.

Underlying flow patterns. The right panels in Fig. 1 show contours for the same pattern as those for the left panels but *without* the underlying axisymmetric contribution. The resulting "reduced" flow pattern of WVF_{39} in Fig. 1(a) appears quite regular, indicating the existence of the dominant wavy mode with $m = 39$ in the

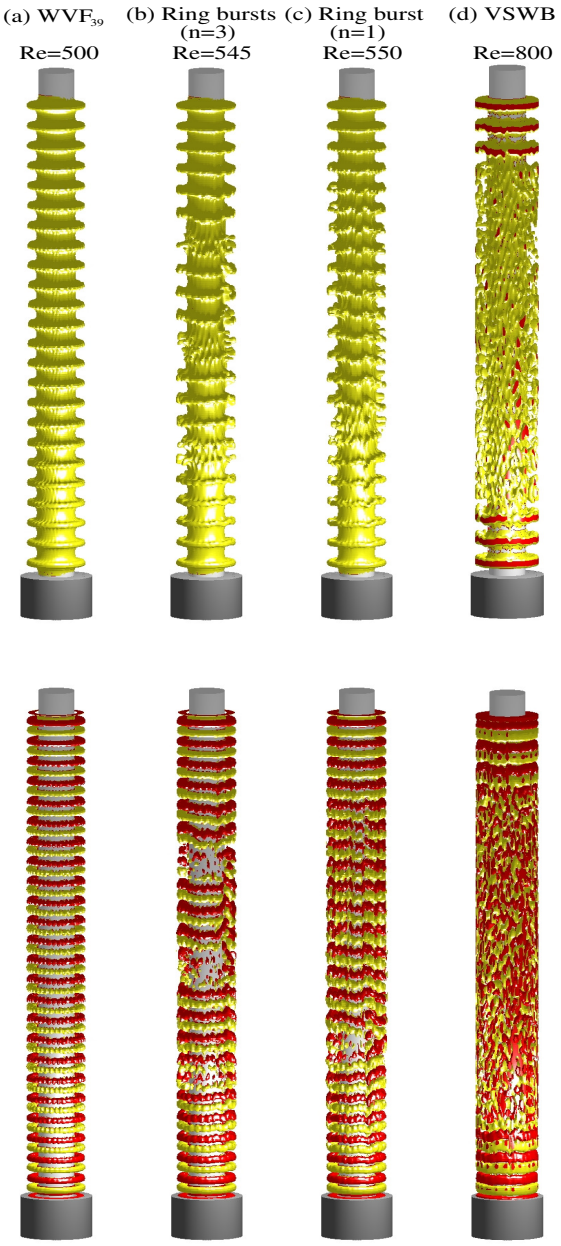

FIG. 2: (Color online) **Angular momentum and vorticity.** Isosurfaces of rv (top row) and η (bottom row) for flows at different values of Re (isolevels shown for the top and bottom rows are $rv = 80$ and $\eta = \pm 30$, respectively). For clear visualization, here and in all following three-dimensional plots the radius ratio is scaled by the factor 100.

azimuthal direction. The black curves in the vertical direction represent the zero contour lines. At several azimuthal positions, these lines narrow, indicating the emergence of a second but weaker mode, e.g., $m = 8$. For order 3 ring bursts, the flow patterns near the lids are somewhat modified due to the presence of higher m modes, as shown in Fig. 1(b). The flow patterns in the central region (including that containing the three ring bursts) exhibit a completely different behavior. In particular, with respect to contours $\eta(m \neq 0)$ the turbulent ring bursts and the separating WVF_{39} pattern appear *indistinguishable*. This finding suggest a quite strong axisymmetric dominance of the flow even when ring bursts arise, confirming that the bursting structure is ordered in azimuthally closed rings around the cylinder with the same $m = 0$ axisymmetry. For turbulent flows or VSWBs in Fig. 1(c), none of the patterns has such an ordered structure.

III. CHARACTERIZATION OF RING BURSTS

A. Angular momentum, azimuthal vorticity, and modal kinetic energy

Figure 2 shows the isosurfaces of the angular momentum rv (top row) and azimuthal vorticity η (bottom row) for representative flow patterns at different values of Re. The dominant axisymmetric contribution and high azimuthal wavenumber associated with WVF_{39}, as shown in Fig. 2(a), serve as the background pattern for ring bursts and VSWBs. The three turbulent, azimuthally closed burst regions associated with the order-3 ring burst pattern is distinctly visible, as shown in Fig. 2(b). Within each burst region, both rv and η appear random but the (background) flow patterns in between the bursting regions are remnant of the WVF_{39} pattern. With increasing Re higher m modes emerge, but the separation between burst and non-burst regions persists. For high values of Re, VSWBs arise, as shown in Fig. 2(d). In this case, isosurface plots of rv and η exhibit random flow patterns except for the regions near the lids due to the Ekman boundary layers.

To better visualize and illustrate the similarity and differences between ring burst and VSWB patterns, we present in Fig. 3 the behaviors of the angular momentum (top panels) and azimuthal vorticity (bottom panels) for a segment of the bulk flow. The length of the segment is $\Gamma/10$. We see that, for the ring burst pattern (left column), there is a dominant axisymmetric component, but this is lost for VSWB. While the entire structure of the ring-burst pattern possesses an axisymmetry due to its azimuthal dominance ($m = 0$), no apparent symmetry exists in the interior of the burst regions. There are thus two distinct spatial scales associated with ring bursts: a large scale determined by the axisymmetry and a small scale present in the interior of the bursting regions.

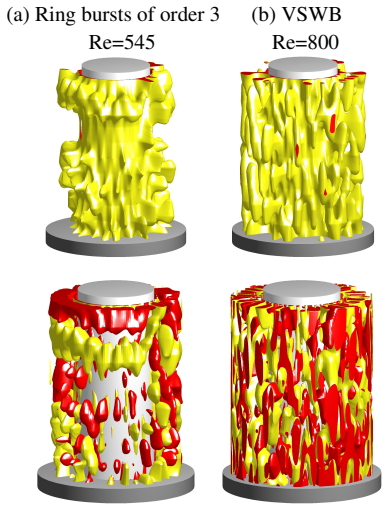

FIG. 3: (Color online) **Three-dimensional views of angular momentum and vorticity.** Magnitude of the angular momentum (top panels) and azimuthal vorticity (bottom panels) for a flow segment of vertical length $\Gamma/10$ for ring bursts (left column) and VSWB (right column). The segment is taken from the region containing the middle ring burst in Fig. 2(b).

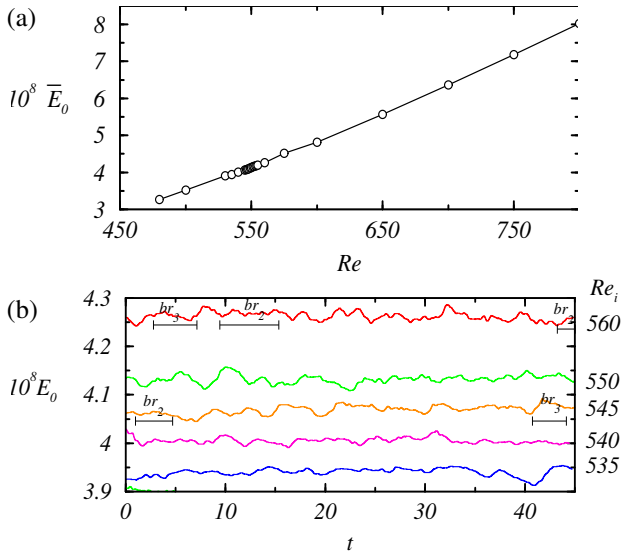

FIG. 4: (Color online) **Behaviors of the kinetic energy.** (a) Time-averaged ($\approx$ 50 diffusion time) axisymmetric energy $\overline{E}_0$ versus Re and (b) time series of E_0 for a number of representative values of Re. The time intervals in which distinct ring-burst patterns last are indicated. For example, for $Re = 560$, ring burst pattern of order 3 is present for $2.5 < t < 6.9$, and that of order 2 can be found for $9.2 \lesssim t \lesssim 15.8$ and $42.6 \lesssim t \lesssim 47.1$. For $Re = 545$, order-2 ring burst pattern appears for $0.5 \lesssim t \lesssim 4.5$ and the order-3 pattern is present for $40.3 \lesssim t \lesssim 44$. However, the ring burst patterns are not reflected in $\overline{E}_0(t)$.

We next examine the modal kinetic energy defined as

$$E := \sum_m E_m = \int_0^{2\pi} \int_0^{\Gamma} \int_{r_i}^{r_o} \mathbf{u}_m \mathbf{u}^*{}_m r dr dz d\theta, \qquad (3)$$

where $\mathbf{u}_m$ ($\mathbf{u}^*{}_m$) is the m-th (complex conjugated) Fourier mode of the velocity field. Due to time dependence of the solutions it is necessary to calculate the time averaged kinetic energy $\overline{E}$. In the energy characterization local quantities such as the radial velocity at mid-height and mid-gap, $u_r(d/2, 0, \Gamma/2, t)$, are relevant.

Figures 4(a) and 4(b) show the time-averaged axisymmetric energy $\overline{E}_0$ versus Re and its time evolutions for a number of representative Re values, respectively. We see that $\overline{E}_0$ increases monotonously with Re, regardless of the nature of the bulk flow patterns. Likewise the time evolution of the kinetic energy presents no clear indication of ring burst patterns. For example, for $Re = 545$, in the time interval $[40, 44]$ the flow pattern should be order-3 ring burst, but the energy time evolution does not show any signature of this burst pattern.

Figures 5(a) and 5(b) show the power spectral density (PSD) of the radial velocity profile at the midgap for WVF and ring burst, respectively. We see that the PSD associated with the ring burst pattern (b) indicates the existence of significantly higher modes than the WVF pattern (a). In fact, the PSD of WVF_{39} in (a) shows a strong peak at the frequency of about 19, which corresponds to the dominant azimuthal mode ($m = 39$). This peak is still present in (b) but it is much broadened, indicating WVF as the background flow pattern for the ring burst. Figure 5(c) shows the scaled PSD curves for several flow patterns for different values of Re. We see that the PSD curves for the ring-burst patterns essentially collapse into one frequency band, but the PSD curve associated with WVF_{39} lies slightly below those of ring burst patterns. There is relatively large difference for small frequencies but it becomes insignificant for higher frequencies. This is further support for the role of WVF_{39} in providing the skeleton structure for all ring burst patterns.

B. Cross-flow energy

From Fig. 4(b), we see that the modal kinetic energy is not effective at distinguishing ring bursts from other basic flow patterns. A suitable and commonly used quantity in the study of fluid turbulence is the so-called cross-flow energy, where typically small values indicate a flow being laminar, large values corresponding to turbulence.

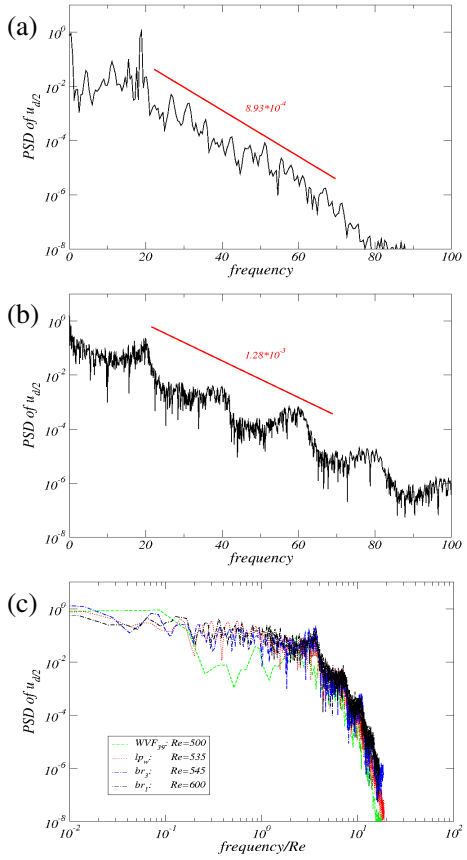

FIG. 5: (Color online) **Power spectral density (PSD).** PSD curves calculated from the radial flow component $u_{d/2} = u(d/2, 0, \Gamma/2, t)$ for (a) WVF_{39} ($Re = 500$) and (b) ring burst of order 3 for $Re = 545$. (c) PSD curves scaled by the respective Reynolds number for different flow patterns. As the number of ring bursts is increased, the local peaks in the PSD curves become more pronounced.

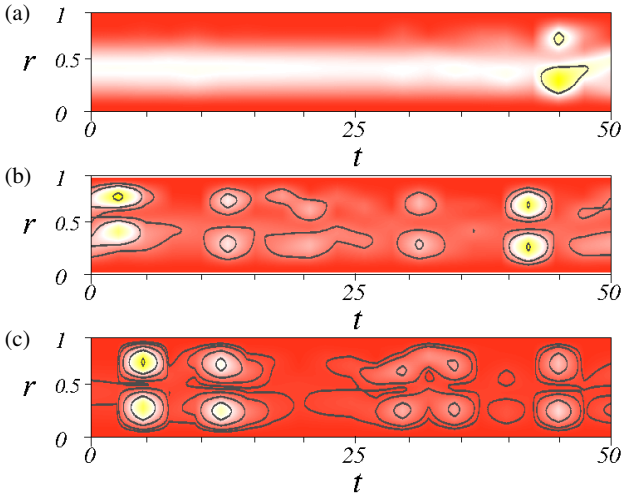

FIG. 6: (Color online) **Radial component of cross-flow energy.** Spacetime plots of the radial component of the cross-flow energy, $E^{cf,r}(r,t) = \langle u_r^2 + u_z^2 \rangle_{A(r)}$, averaged over the surfaces A of a concentric cylinder at radius r for (a) $Re = 500$, (b) $Re = 545$, and (c) $Re = 560$. Red (yellow) color indicates high (low) energy with contours defined as $\Delta E^{cf,r} = 5 \times 10^5$. The maximum energy values in (a-c) are approximately 8.1×10^5, 8.5×10^6, and 1.2×10^6, respectively. For better visualization the radial gap width is magnified by a factor of 500 (the same for Fig. 7 below).

1. *Radial component of cross-flow energy*

The radial component of the cross-flow energy is given by [27]

$$E^{cf,r}(r,t) = \langle u_r^2 + u_z^2 \rangle_{A(r)}, \tag{4}$$

where $\langle \cdot \rangle_{A(r)}$ denotes averaging over the surface of a concentric cylinder at radius r. The cross-flow energy component $E^{cf,r}(r,t)$ measures the instantaneous energy associated with the radial and axial velocity components at radial distance r. Figure 6 shows the spacetime plots of $E^{cf,r}(r,t)$ over the time period of 50 DT for three values of Re. We observe the temporal emergence and disappearance of various ring-burst patterns in the bulk. For example, for $Re = 545$, the order-3 ring burst pattern exists for $40 \le t \le 44$, and the order-2 pattern appears for $0.5 \le t \le 4.5$, as shown in Fig. 6(b). For $Re = 560$, an order-3 pattern appears for $2.5 \le t \le 7.0$, and a single ring burst pattern (order 1) exists for $43 \le t \le 47$, as shown in Fig. 6(c).

Plots of the cross-flow energy exhibit two features. Firstly, presence of the order-1 ring burst pattern is accompanied by a significant increase in the radial cross-flow energy as compared with that associated with the background flow, e.g., WVF_{39}, as indicated by the uniform red (dark gray) regions. Secondly, the profile of $E^{cf,r}(r,t)$ for any ring burst pattern is approximately symmetric with respect to the middle of the gap. It is thus plausible that the ring-burst patterns are similar to the so-called *turbulent WVF* state [22, 28–30] (see Sec. III C). The symmetry may be a consequence of the quasi two-dimensional nature of the flow. In all cases, the occurrence of ring burst patterns enhances the magnitude of the cross-flow energy.

Figure 7(a) shows a magnification of a segment of Fig. 6(b) for $t \in [0, 1.8]$, which contains the emergence and disappearance of order-3 ring burst for $Re = 545$, occurring at $t \approx 0.45$ and $t \approx 1.35$, respectively. Outside this time interval the flow is WVF_{39}, which constitutes a nearly uniform background without any significant variation in $E^{cf,r}(r,t)$. The spatial distribution of $E^{cf,r}(r,t)$ exhibits a kind of symmetry about $r = 0.5$. Figure 7(b) shows the average cross-flow energy, $\langle E^{cf,r} \rangle_r$, as a function of time t, corresponding to the emergence and disap-

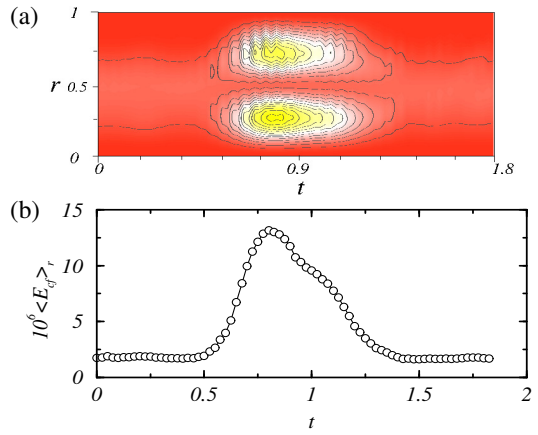

FIG. 7: (Color online) **Magnified view of the radial component of the cross-flow energy.** (a) Magnification of a segment of Fig. 6(b) for $t \in [0, 1.8]$ illustrating the emergence and disappearance of order-3 ring burst pattern for $Re = 545$. The contours are defined through $\Delta E^{cf,r} = 5 * 10^5$, and the maximum energy value is about 8.288×10^6. (b) Averaged radial cross-flow energy $\langle E^{cf,r} \rangle_r$ versus t for order-3 ring burst for $Re = 545$. The nearly constant background flow is WVF_{39} with $\langle E^{cf,r}(\mathrm{WVF}_{39}) \rangle_r \approx 2 \times 10^{-6}$.

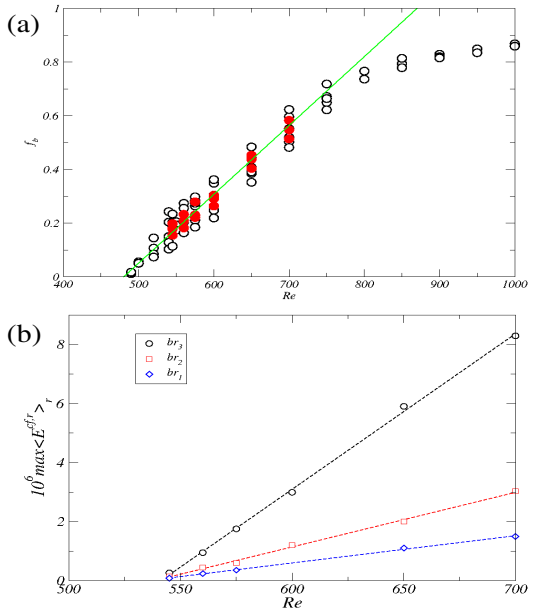

FIG. 8: (Color online) **Onset of burst patterns.** (a) Burst fraction f_b as a function of Re. A linear fit indicates that onset of VSWBs occurs for $Re \approx 480$ (the experimental onset [14] is $Re \approx 483$). (b) The maximum average radial energy $\langle E^{cf,r} \rangle_r$ [Eq. (4)] versus Re for ring bursts of different order ($n \in \{1, 2, 3\}$). The linear behavior suggests that ring bursts are result of a forward bifurcation, the onset of which occurs for $Re_c \approx 537$. In this figure, the average energy of the underlaying background flow, $\langle E^{cf,r} \rangle_r$, has been subtracted off.

pearance of the ring burst pattern. We observe a significant enhancement of the average radial energy over that of the background flow ($\langle E^{cf,r} \rangle_r \approx 2 \times 10^{-6}$. In fact, in the time interval where the ring burst exists, the maximum value of the average radial energy is about one order of magnitude larger than that of the background flow. In general, the maximum energy depends on the number n (order) of ring bursts in the annulus, where a larger value of n corresponds to larger value of the maximum energy.

The emergence and development of any type of burst patterns with increasing Re can be conveniently characterized using the quantity f_B, the percentage of the annulus showing bursts in the spacetime plot. Figure 8(a) shows f_B versus Re, where we observe approximately a linear behavior for $Re \lesssim 900$, and the transition to bursts occurs for $Re \approx 480$, in agreement with the onset of VSWB [14]. Onset of ring bursts can be revealed by examining the maximum value of the average radial energy, $\langle E^{cf,r} \rangle_r$, versus Re, as shown in Fig. 8(b). Regardless of the order n of ring bursts, there is a linear increase in $\langle E^{cf,r} \rangle_r$ with Re, suggesting a type of forward bifurcation. Calculations of the flow amplitudes show a square-root type of scaling behavior with increasing parameter difference from the "critical" point, providing further support for the forward nature of the bifurcation. Due to strong localization of the ring bursts, the slope of the linear scaling behavior depends on the ring-burst order n. Nonetheless, the onset value $Re_c \approx 537$ of ring bursts does not depend on n. This is evidence that ring bursts emerge *after* VSWBs.

2. *Axial component of cross-flow energy*

The axial component of the cross-flow energy is

$$E_m^{cf,z}(z,t) = \langle (u_r)_m^2 + (u_z)_m^2 \rangle_{A(z)}. \qquad (5)$$

where $A(z)$ stands for averaging over the radial and azimuthal variables on the surface of a disc at a fixed axial position z. Figure 9 shows the time-averaged value $\overline{E}_m^{cf,z}$ for the order-3 ring burst pattern for different azimuthal modes. The axisymmetric component $\overline{E}_0^{cf,z}$ is dominant. Near the center of the ring burst region in the axial direction, the values of $\overline{E}_0^{cf,z}$ are smaller than those around the edges. However, the contributions from all higher modes, i.e., $\overline{E}_m^{cf,z}$ for $m > 0$, have similarly small magnitudes as compared with $\overline{E}_0^{cf,z}$, as shown in Fig. 9(b). In fact, for higher m modes, the axial components of their cross-flow energies are randomly distributed over z and they are not indicators of any appreciable difference between the background flow and the ring burst pattern.

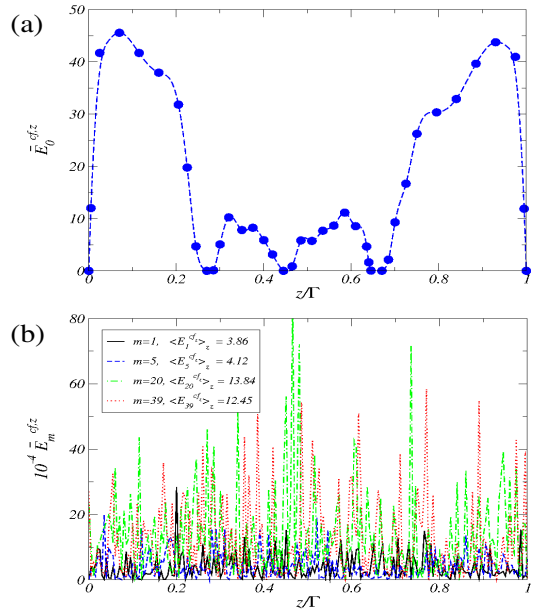

FIG. 9: (Color online) **Axial component of cross-flow energy.** Associated with the order-3 ring burst pattern for $Re = 545$, (a) time averaged axisymmetric energy component $\overline{E}_0^{cf,z}$ and (b) energy contributions $\overline{E}_m^{cf,z}$ from selected higher azimuthal m modes. In (b), additional axial average energy values are indicated.

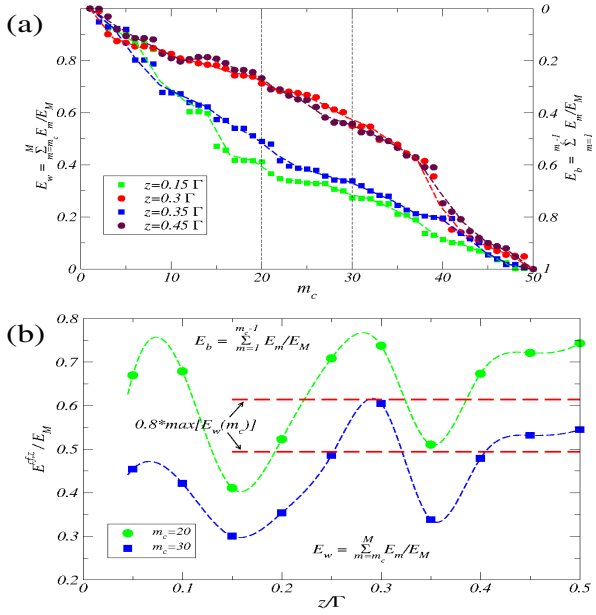

FIG. 10: (Color online) **Characterization of axial cross-flow energy based on mode separation.** (a) Variation of the axial cross-flow energy component $E_m^{cf,z}(z) = E_b^{cf,z}(z) + E_w^{cf,z}(z)$ versus the cutoff wavenumber m_c for two axial positions in the burst region ($z = 0.3\Gamma$ and 0.45Γ, circles) and in the background region ($z = 0.15\Gamma$ and 0.35Γ, squares). (b) Spatial variations of $E_b^{cf,z}(z) = \sum_{m=1}^{m_c-1} E_m^{cf,z}(z)$ and $E_w^{cf,z}(z) = \sum_{m=m_c}^{M} E_m^{cf,z}(z)$ with z for $m_c = 20$ (circles) and 30 (squares). Regions above (below) each curve indicate E_b (E_w). The two horizontal dashed lines give the 80% threshold of the maximum values of $[E_w(m_c = 20)]$ (lower) and $[E_w(m_c = 30)]$ (upper), respectively. In the calculations the zero mode contribution is excluded. Due to normalization with E_M the sum must be unity.

3. *Mode separation of axial cross-flow energy*

To better characterize the ring-burst patterns in relation to the background wavy-like and general burst patterns, we devise a method based on the idea of mode separation. Since a burst pattern includes modes of higher azimuthal wave numbers, we can decompose the axial component of the cross-flow energy $E_m^{cf,z}(z,t)$ into two distinct subcomponents:

$$E_w^{cf,z}(z)+E_b^{cf,z}(z) = \sum_{m=1}^{m_c-1} E_m^{cf,z}(z)+\sum_{m=m_c}^{M} E_m^{cf,z}(z), \quad (6)$$

where $E_w^{cf,z}(z)$ and $E_b^{cf,z}(z)$ denote the axial components of the cross-flow energy associated with the background wavy-like and burst patterns, respectively, and m_c is some cutoff mode number. Note that the axisymmetric component of the cross-flow energy is excluded because it is significantly larger than all other components [Figs. 9(a,b)]. We choose the normalization factor to be the total cross-flow energy for all modes except $m = 0$:

$$E_M^{cf,z} = \sum_{m=1}^{M} E_m^{cf,z}. \quad (7)$$

Figure 10(a) shows the basic E_w and the burst contribution E_b at different axial positions versus the cutoff wavenumber m_c. We observe that the curves for z positions within the burst region (circles, e.g, at $z = 0.3\Gamma$ and0.45Γ, Figs. 1 and 9) are higher than those in the wavy-like background (squares, e.g., at $z = 0.15\Gamma$ and 0.35Γ), where the former exhibit a rapid decrease in the energy to collapse with the latter for m_c about 39. The variations of E_b and E_w along the annulus length for two different cutoff wavenumbers [$m_c = 20, 30$, as indicated by the vertical lines in Fig. 10(a)] are shown in Fig. 10(b). Neglecting the differences in their magnitudes, the variations show qualitatively similar behaviors. Using a cutoff level with 80% of the maximum of the background contribution $[E_w(m_c)]$, we find a good agreement with the visible energy thresholds between the background and burst regions (cf. Fig. 1). We thus see that, through some proper choice of the cutoff mode number, the burst and non-burst regions can be distinguished by examining the axial cross-flow energy variations associated with the cutoff mode.

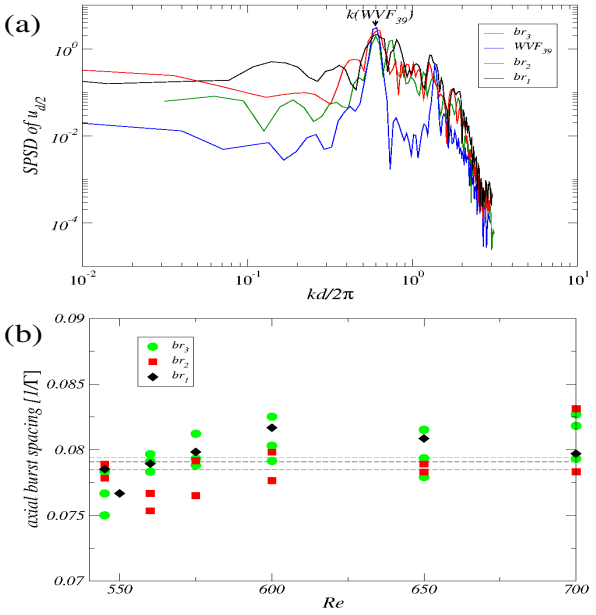

FIG. 11: (Color online) **Axial spacing of ring bursts.** (a) SPSD of the radial velocity u_r at the midgap for $Re = 545$, where k is the axial wave number. (b) Axial spacing of the burst regions for order-n ring bursts ($n \in \{1, 2, 3\}$), indicated by the horizontal lines. The average spacing is about 0.079, the axial spacing of two pairs of Taylor vortices constituting four vortex cells.

C. Axial spacing and localization

The axial ranges of distinct ring burst regions are approximately identical. Figure 11(a) shows the spatial power spectral density (SPSD) of the radial velocity u_r along a line at the midgap in the center of the bulk for the background flow and three types of ring-burst patterns. We observe that the four curves coincide at the first sharp peak determined by the wave number associated with the background flow WVF_{39} that consists of 24 vortex pairs in the axial direction. The corresponding axial wavelength and wave number are $\lambda \approx 1.667$ and $k \approx 3.770$, respectively. In addition, several broadband peaks at higher wave numbers exist in the SPSD of the ring burst patterns, corresponding to a number of short wavelength bursts within the respective patterns. The broadband nature at higher wave numbers are indicative of dominance of small-scale burst patterns. Figure 11(b) shows the axial spacing associated with various ring burst patterns as a function of Re, where each horizontal dashed line represents the averaged axial spacing for a particular ring burst pattern. The axial spacing is apparently independent of the value of Re and of the order n of the ring-burst pattern. The typical value of axial expansion agrees well with the axial dimension of two-pair Taylor vortices that constitute four single vortex cells, which holds for all ring-burst flows that we have succeeded in uncovering. Analogous to the behavior of the cross-flow energy, this behavior is indicative of that of turbulent WVFs [22, 28–30]. We note that the size of only one pair of Taylor vortices (two cells) is too small to account for the observed range of axial expansion. This is consistent with the formation process of ring bursts. In particular, any localized turbulent patch, after its generation, first expands in the axial direction (to four cells) before growing in the azimuthal direction. Whenever the burst region has expanded to a larger size in the axial direction, the closed ring structure is destroyed, leading to VSWBs.

IV. CONCLUSIONS AND DISCUSSIONS

This paper provides a comprehensive numerical study of the quasi two-dimensional Taylor-Couette systems of radius ratio close but not equal to unity, a regime that has not been studied previously. The relevant control or bifurcation parameter is the Reynolds number Re. For small Re values, TVF initially arises near one of the lids in a single cell, extends and finally fills the bulk interior completely. As Re is increased the TVF loses its stability and WVF emerges through a supercritical Hopf bifurcation. WVFs with high azimuthal wavenumbers, e.g., $m = 39$, constitute a persistent background flow, on top of which more complex flow structures develop, such as VSWBs that has been experimentally observed [14].

The main result of this paper is the discovery of a new type of transient, intermittent state *en route* to turbulence with increasing Re: ring bursts. They emerge when localized turbulent patches grow and close azimuthally, signifying a higher order instability. The ring bursts occur in various orders and the azimuthally closed burst regions possess axial expansion surrounded by the WVF background flow or more complex flows at high Re values. The ring burst patterns differ characteristically from the localized VSWB turbulent patches. The axial expansion of ring burst patterns of different orders correlates well with the size of the double-pair Taylor vortex structure, providing plausible reason that the patterns are similar to the turbulent WVF structure [22, 28–30] that usually occurs through the whole annulus at higher Reynolds numbers. We develop a mode separation method based on decomposing the cross-flow energy to distinguish between burst and non-burst patterns, where the former and latter are associated with higher and lower azimuthal modes, respectively. We also find that the radial cross-flow energy changes significantly in the presence of ring burst patterns. By examining the maximum value of

the cross-flow energy, we determine the onset of the ring-burst patterns at the critical Reynolds number of $Re_c \approx 537$, which is larger than that for the onset of VSWBs [14] (about 482). For ring burst patterns of different orders, their expansions in the axial direction are nearly identical, and they tend to shift along the axial direction.

There are a number of differences between turbulence in the wide-gap (e.g., radius ratio 0.5 to 0.8) and narrow-gap (e.g., radius ratio 0.99) Taylor-Couette systems. Firstly, in the wide-gap case, the intensity distributions of turbulent fluctuations are often uneven in the radial direction [22, 27], where more energetic turbulent fluctuations occur towards the inner cylinder wall. The regions near the inner cylinder thus exhibits stronger turbulence than in the region near the outer cylinder. This radial dependence of turbulent fluctuations is lost in the quasi two-dimensional, narrow-gap Taylor-Couette system, where turbulence is observed through the bulk in the radial direction. Secondly, in wide-gap systems, phenomena such as turbulent streaks [22], small-scale Görtler vortices and herringbone-like streaks [23] can occur near both inner and outer cylindrical walls. Examining the typical size of the small Görtler vortices [23] reveals that, in the narrow-gap case these vortices have expansion larger than the radial width, excluding the possibility of generating turbulent streaks from small-scale Görtler vortices. Indeed, our simulations do not reveal any kind of such small scale vortices. This might explain the loss of radial dependence of turbulence, as can be seen, e.g., from the cross-flow energy behavior in Fig. 6. The mechanism that generates turbulence in quasi two-dimensional Taylor-Couette system is thus quite different from that in the three-dimensional system. In fact, in narrow-gap systems turbulence emerges at the boundary layer of the neighboring vortex cells almost immediately at any radial position.

Turbulence in quasi two-dimensional Taylor-Couette systems has different features than those in the planar systems as well. In particular, firstly, in planar Couette flows there is a significant difference between the velocities at the two walls, and asymmetry in the intensity distribution of turbulent fluctuations is caused by the curvature effect. In the narrow-gap case, this difference is minimal. Secondly, while there are ring burst patterns of turbulent bands in planar Couette flows [31**?**], the background flow is laminar, versus wavy-like patterns in quasi two-dimensional systems, where the former defines a threshold between basic state and turbulence but the latter is a threshold between an already complex state and turbulence. Except this difference there is in fact a remarkable similarity between turbulence in both types of systems. For example, detailed investigations [31] of the laminar-turbulent boundary layer in planar Couette flows revealed isolated band states of turbulence in confined domains close to the global stability threshold. Although these bands appear at various different angles, they are all parallel, which are remarkably analogous to our ring-burst patterns on an unrolled cylindrical surface (e.g., comparing Fig. 1 with Figs. 1 and 11 in Ref. [**?**]). In addition, the routes to turbulence are similar: in both cases the turbulent bands grow out of a small localized turbulent spot that subsequently expands in some direction.

It may be challenging to detect ring-burst patterns experimentally as they coexist with other complex states such as VSWBs with similar turbulent characteristics. Nonetheless, given that the Taylor-Couette system is a paradigm enabling well controlled experiments on complex vortex dynamics and turbulence, we hope our finding will stimulate further research of turbulence in quasi two-dimensional regime of the system, a regime that has received little attention in spite of a large body of literature on Taylor-Couette flows in general.

Acknowledgments

Y. D. was supported by Basic Science Research Program through the National Research Foundation of Korea (NRF) funded by the Ministry of Education, Science and Technology (NRF-2013R1A1A2010067). Y.-C. L. was supported by AFOSR under Grant No. FA9550-12-1-0095.

[1] A. N. Kolmogorov . Proc. R. Soc. Lond. A **434**, 9 (1994).
[2] R. H. Kraichnan and D. Montgomery . Rep. Progr. Phys. **43**, 547 (1980).
[3] M. Lesieur *Turbulence in Fluids.* 2nd ed. (Kluwer, Dordrecht, 1990).
[4] D. G. Dritschel and B. Legras . Phys. Today **46**, 44 (1993).
[5] D. W. Waugh, R. A. Lamb, R. J. Atkinson, M. R. Schoeberl, L. R. Lait, P. A. Newman, M. Lowenstein, D. W. Toohey, L. M. Avallone, C. R. Webster and R. D. May . . Geophys. Res. **99**, 1071 (1994).
[6] U. Frisch *Turbulence.* (Cambridge Univ. Press, Cambridge, UK, 1996).
[7] J. P. Gollub and H. L. Swinney . Phys. Rev. Lett. **35**, 927 (1975).
[8] J. P. Gollub and S. V. Benson . J. Fluid Mech.**100**, 449

(1980).
[9] G. I. Taylor . Philos. Trans. R. Soc. London A **223**, 289 (1923).
[10] D. Coles . J. Fluid Mech. **21**, 385 (1965).
[11] H. A. Snyder . J. Fluid Mech. **35**, 337 (1969).
[12] R. C. DiPrima and H. L. Swinney *Hydrodynamic instabilities and the transition to turbulence.* (Springer, Berlin, 1985) pp. 139–180.
[13] C. D. Andereck, S. S. Liu and H. L. Swinney . J. Fluid Mech. **164**, 155 (1986).
[14] C. S. Carey, A. B. Schlender and C. D. Andereck . Phys. Rev. E **75**, 015303 (2007).
[15] R. Tagg . Nonlinear Science Today **4**, 1 (1994).
[16] P. Chossat and G. Iooss *The Couette-Taylor Problem.* (Springer, Berlin, 1994).
[17] K. Coughlin and P. S. Marcus . Phys. Rev. Lett. **77**, 2214 (1996).
[18] S. Altmeyer and C. Hoffmann . New J. Phys. **12**, 113035 (2010).
[19] H. Faisst and B. Eckhardt, . Phys. Rev. E **61**, 7227 (2000).
[20] P. R. Fenstermacher, H. L. Swinney and J. P. Gollub . J. Fluid Mech. **94**, 103 (1979).
[21] P. Colovas and C. D. Andereck . Phys. Rev. E **55**, 2736 (1996).
[22] S. Dong . J. Fluid Mech. **587**, 373 (2007).
[23] H. Görtler . ACA Tech. Memo. , 1375 (1954).
[24] S. Hughes and A. Randriamampianina . Int. J. Heat Fluid Flow **28**, 501 (1998).
[25] M. Avila, M. Grimes, J. M. Lopez and F. Marques . Phys. Fluids **20**, 104104 (2008).
[26] S. Altmeyer, Y. Do, F. Marques, and J. M. Lopez . Phys. Rev. E **86**, 046816 (2012).
[27] H. J. Brauckmann and B. Eckhardt . **87**, 033004 (2013).
[28] Y. Tseng and J. Ferziger . Int. J. Heat Fluid Flow **5**, 034 (2004).
[29] N. Ohmura, T. Makino, A. Motomura, Y. Shibata and K. Kataoka . Int. J. Heat Fluid Flow **19**, 159 (1998).
[30] S. Dong . Phys. Rev. E **77**, 035301(R) (2008).
[31] D. Barkley and L. S. Tuckerman . Phys. Rev. Lett. **94**, 014502 (2000).
[32] L. S. Tuckerman and D. Barkley . Phys. Fluids **23**, 041301 (2011).